

The X-ray spectral evolution of Cyg X–2 in the framework of bulk Comptonization

R. Farinelli¹, A. Paizis², R. Landi³ & L. Titarchuk^{1,4}

¹ Dipartimento di Fisica, Università di Ferrara, Via Saragat 1, 44100 Ferrara, Italy

² INAF-IASF, Sezione di Milano, Via Bassini 15, 20133 Milano, Italy

³ INAF-IASF, Sezione di Bologna, Via Gobetti 1, 40100, Bologna, Italy

⁴ NASA/GSFC, Greenbelt, MD 20771

Preprint online version: June 22, 2021

ABSTRACT

Context. The interplay of thermal and bulk motion Comptonization to explain the spectral evolution of neutron star LMXBs including transient hard X-ray tails is gaining a strong theoretical and observational support. The last momentum has been given by the advent of a new XSPEC Comptonization model, COMPTB, which includes thermal and bulk Comptonization.

Aims. We used COMPTB to investigate the spectral evolution of the neutron star LMXB Cyg X–2 along its Z-track. We selected a single source in order to trace in a quantitative way the evolution of the physical parameters of the model.

Methods. We analyzed archival broad-band *BeppoSAX* spectra of Cyg X–2. Five broad-band spectra have been newly extracted according to the source position in the Z-track described in the color-color and color-intensity diagrams.

Results. We have fitted the spectra of the source with two COMPTB components. The first one, with bulk parameter $\delta=0$, dominates the overall source broad-band spectrum and its origin is related to thermal upscattering (Comptonization) of cold seed photons off warm electrons in high-opacity environment. We attribute the origin of these seed photons to the part of the disk which illuminates the outer coronal region (transition layer) located between the accretion disk itself and the neutron star surface. This thermal component is roughly constant with time and with inferred mass accretion rate. The second COMPTB model describes the overall Comptonization (thermal plus bulk, $\delta > 0$) of hotter seed photons which come from both the inner transition layer and from the neutron star surface. The appearance of this component in the colour-colour or hardness-intensity diagram is more pronounced in the horizontal branch and is progressively disappearing towards the normal branch, where a pure blackbody spectrum is observed.

Conclusions. The spectral evolution of Cyg X–2 is studied and interpreted in terms of changes in the innermost environmental conditions of the system, leading to a variable thermal-bulk Comptonization efficiency.

Key words. stars: individual: Cyg X–2 — stars: neutron — X-rays: binaries — accretion, accretion disks

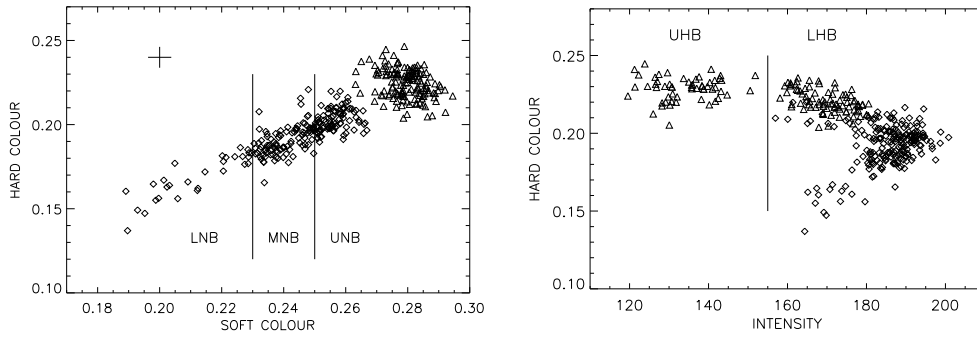


Fig. 1. Color-color diagram (*left panel*) and hardness intensity diagram (*right panel*) of Cyg X-2 during the 1996 (*triangles*) and 1997 observation (*diamonds*). The hard colour is defined as the 7–10.5 keV/4.5–7 keV bands count rate ratio while the soft colour is defined as the 4.5–7 keV/1.4–4.5 keV count rate ratio. For the hardness intensity diagram, the intensity is given by the 1.4–10.5 keV count rate. A typical error bar is shown in the left panel. The regions of the branches for which particular spectral analysis was carried-out are also shown.

1. Introduction

The bright persistent Low Mass X-ray Binary (LMXB) Cyg X-2 is one of the Galactic sources hosting a neutron star (NS) which belong to the Z class, due to the Z-shape it displays in its color-color (CD) and hardness-intensity diagram (HID). The parts of the diagram are referred to as the horizontal branch (HB) at the top of the Z, the normal branch (NB) along the diagonal, and the flaring branch (FB) at the base of the Z diagram. Actually, Z sources move continuously along this diagram and the position of the source within the Z is believed to be related to the mass accretion rate that increases from the HB, lowest accretion, to the FB, highest accretion (Hasinger et al. 1990).

The <20 keV X-ray spectrum of Cyg X-2, and of persistent bright NS LMXBs in general, has been usually described as the sum of a soft and a hard component. The soft component is interpreted as emission from the accretion disc (Eastern model, Mitsuda et al. 1984) or originating at (or close to) the NS (Western model, White et al. 1986) whereas the hard component is most likely formed due to Comptonization of NS and/or disc emission by a hot plasma (so-called "corona") electrons. These two models describe equally well the spectra of NS LMXBs below about 20 keV. The first studies of the Cyg X-2 X-ray spectrum above ~ 20 keV were performed with detectors on balloons (Peterson 1973). Interestingly, an unexpected hardening was observed in the spectrum of Cyg X-2 that was fitted by a powerlaw (PL) with photon index of 2.8 (Maurer et al. 1982) or 1.9 (Ling et al. 1996). It soon became clear that simultaneous broad band observations of the X-ray spectrum were needed to investigate the nature of this spectral flattening.

The advent of broad-band X-ray missions, such as *BeppoSAX*, *RXTE*, *INTEGRAL*, revealed that many such spectral hardenings (so-called "hard tails") occur in Z sources: Cyg X-2 (Frontera et al. 1998; Di Salvo et al. 2002), GX 17+2 (Farinelli et al. 2005; Di Salvo et al. 2000), GX 349+2 (Di Salvo et al. 2001), Sco X-1 (D'Amico et al. 2001; Di Salvo et al. 2006), GX 5-1 (Paizis et al. 2005; Asai et al. 1994), GX 340+0 (Lavagetto et al. 2004). Recently, a hard tail has also been dis-

covered in the bright atoll source GX 13+1 (Paizis et al. 2006, hereafter P06).

The spectra of these sources and in particular the hard X-ray tails have been extensively studied and focused on a single source basis, and mainly in terms of phenomenological models (see Barret 2001; Di Salvo & Stella 2002, for a review on NS LMXB spectra). In the attempt to study these sources in terms of a *unified physical scenario* in the less known domain above 20 keV, P06 studied the long term average hard X-ray (>20 keV) spectra of a sample of twelve bright NS LMXBs (six Z and six atoll sources), using data from IBIS instrument on-board *INTEGRAL* (Winkler et al. 2003). Merging their results with those of Falanga et al. (2006) for the atoll source 4U 1728–34 (GX 354–0), P06 identified four main spectral states for NS LMXBs (see Fig. 4 in P06): *low/hard* state (GX 354–0), *hard/PL* state (H 1750–440 and H 1608–55), *intermediate* state (where the hard X-ray tail appears, e.g., Cyg X–2, Sco X–1, GX 5–1, GX 17+2) and *soft* state (e.g., GX 3+1, GX 9+1, GX 9+9). The different spectral states, including the hard tails, could be well fit in terms of the interplay of thermal and bulk Comptonization (TC and BC, respectively) using the BMC model in XSPEC. The relative contribution between the two Comptonization regimes (thermal versus bulk) is proposed to be drawn by the *local* accretion rate \dot{M} . Indeed (see P06), starting from the lowest level \dot{M} , the *low/hard* state spectra, whose cut-off is below 100 keV, can be interpreted in terms of TC of soft photons off a hot (~ 30 keV) electron population; at increasing \dot{M} , bulk Comptonization starts to become relevant with the result of moving at higher energies the cut-off (*hard/PL* state); higher accretion rates lead to high bulk inflow Comptonization efficiency that is seen as an extended hard tail in the spectrum above 30 keV (*intermediate* state). In this state TC becomes less efficient since the coronal plasma is cooled down to ~ 3 keV and the emergent spectrum is dominated by a strong thermal bump (with cut-off energy around 10 keV) with overlapped a high-energy PL-like tail up to 100 keV; finally, the *soft* state spectra, with highest \dot{M} , are described by a single TC component (the “bump”) with a low- kT_e and high- τ plasma, as expected in a high \dot{M} environment. The emission above 30 keV is no longer present since the high local pressure gradient either prevents matter to reach the NS or strongly decelerates it¹.

The study of the average spectra of the twelve NS LMXBs above 20 keV allowed P06 to present a qualitative scenario for the X-ray spectral evolution of these sources along with the radio - X-ray connection. Nevertheless, the lack of data below 20 keV prevented the authors from drawing more stringent conclusions on the accretion geometry of the systems and on the physical parameters. To overcome these limitations and to obtain a quantitative view of the parameter evolution within a single source we present the study of the broad-band (0.4–120 keV) *BeppoSAX* spectra of Cyg X–2 in terms of a newly updated version of the BMC model, hereafter referred to as COMPTB (Farinelli et al. 2008). A similar analysis of *BeppoSAX*, *RXTE* and *INTEGRAL* data from a number of LMXBs has been already made by (Farinelli et al. 2007, 2008, hereafter F07 and F08, respectively).

2. Observations and data analysis

We analyzed two *BeppoSAX* (Boella et al. 1997a) observations of Cyg X–2, the first one performed on 1996 July 23 (00:54:21 to 23:53:06 UT) and the second on 1997 October 26 (15:37:11 UT) to

¹ See P06 for a more detailed description of the X-ray spectral evolution and for the X-ray / radio correlation obtained.

October 28 (04:00:12 UT). This data set has already been presented by Di Salvo et al. (2002, hereafter DS02). In the analysis carried-out by DS02, colour-colour and hardness intensity diagrams (CD and HID, respectively) of the source with the *Medium-Energy Concentrator Spectrometer* (1.8-10 keV; Boella et al. 1997b). were produced. The soft colour (SC) was defined as the 4.5–7 keV/1.4–4.5 keV count rate ratio, while the hard colour by the 7–10.5 keV/4.5–7 keV count rate ratio. On the other hand, in the HID the intensity was defined by the 1.4–10.5 keV count rate. During the 1996 observation, the source was at HB of the CD/HID diagram; this is much more evident using the HID, were two distinct regions separated by a gap around 150 cts s^{-1} are clearly visible (see Fig. 1 here, right hand panel, and Fig. 1 in DS02). These two HB regions were labeled as an upper HB and a lower HB (UHB and LHB, respectively) and two broad-band spectra were separately extracted for each of them. We adopted the same approach. On the other hand, during the 1997 observation, the source was at NB; in this latter case, the NB structure is more evident using the CD. Three spectra were extracted by DS02 for the NB, and they were labeled as an upper NB, a medium NB and a lower LNB (UNB, MNB and LNB, respectively, see Fig. 2, left panel, in DS02). We note however that the time-filters used by DS02 to extract the source spectra of the three parts of the NB were almost rough as they actually simply considered three consecutive time intervals which were associated to the periods spent by the source *on average* at UNB, MNB and LNB stages, respectively. We realize however that this is, in fact, not true as the source motion along the NB is not strictly continuous and smooth but it actually behaves like a random motion; this is clearly evident plotting e.g. the SC as a function of time (see Fig. 2). In order to produce spectra which correspond to *effective* UNB, MNB and LNB positions we thus used a more refined criterion; namely, we also divided the NB in three intervals (see Fig. 1, left panel), according to SC-value being greater than 0.25 (UNB), between 0.23 and 0.25 (MNB) and lower than 0.23 (LNB), but temporal filter for spectral extraction were produced following the source behaviour as reported in Fig. 2.

The shift of the source position in the CD/HID between our plots and those reported in DS02 has two reasons: first, we extracted light-curves (such as energy spectra) from a $4'$ region centered around the MECS source image (while in DS02 no spatial selection was used for producing CD/HID), and second we used a better MECS instrumental channel-to-energy conversion law, required when extracting light curves in different energy bands.

The time-filtered spectra of the high-energy $\widehat{\text{Pho}}\text{swich Detection System}$ (PDS; Frontera et al. 1997) were produced using the XAS package and we grouped the PDS channels in order to have $S/N \gtrsim 3$. Bin with lower threshold, as being statistically meaningless, were discarded and not included in the fit. A further comment is required for the use of the LECS response files (the energy redistribution matrix and the effective area files, RMF and ARF, respectively). When the LECS count rate is about $50\text{--}60 \text{ cts s}^{-1}$ or lower, the standard on-line available response matrix can be safely used, while for higher count rates specific observation-related RMF and ARF files should be produced. The fits on the LECS Crab spectrum ($\sim 200 \text{ cts s}^{-1}$) clearly shows the presence of $\lesssim 5\%$ residuals in the region $0.5\text{--}1 \text{ keV}$ and $2\text{--}3 \text{ keV}^2$. It is thus evident that when a source spectrum is very bright and far from being Crab-like, these instrumental features can be significantly enhanced. This problem may be critical for LMXBs as their low-energy X-ray emission is dominated by the

² See <http://bepposax.gsfc.nasa.gov/bepposax/software/index.html>.

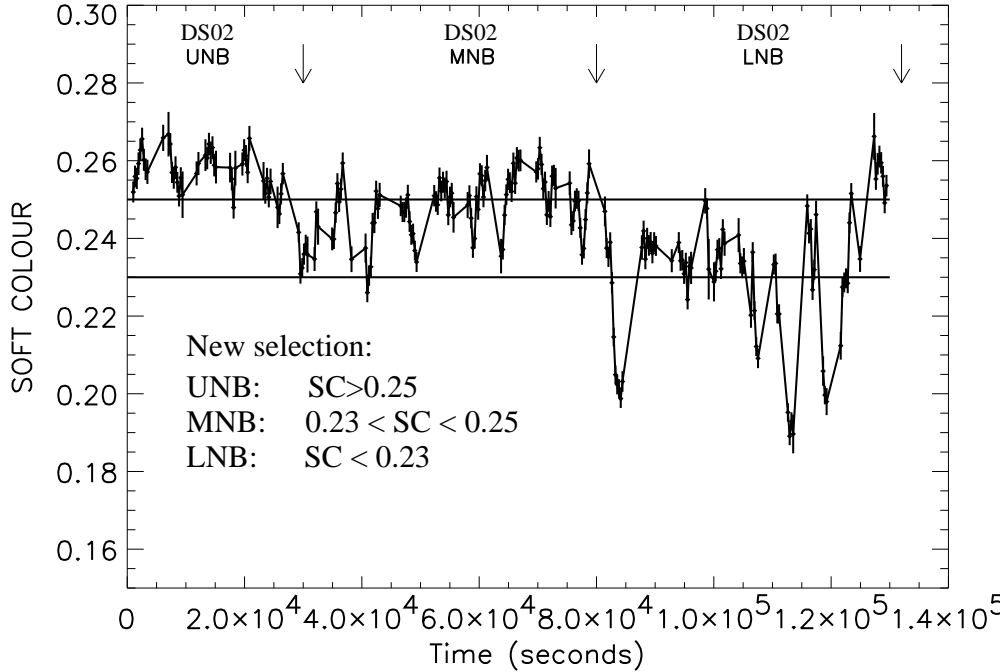


Fig. 2. Temporal evolution of Cyg X-2 soft color in the NB. The three intervals used by DS02 to classify the NB are shown with the upper arrows. The soft color intervals used in this work are given and shown in the horizontal lines.

presence of the soft ~ 0.5 keV BB-like component in addition to photoelectric absorption. The LECS count rate of the 1996 observation (HB spectra) of Cyg X-2 was around 50 cts s^{-1} (~ 0.25 Crab) while during 1997 observation (NB spectra) it was on average $\sim 90 \text{ cts s}^{-1}$ (~ 0.4 Crab). We thus produced new RMF and ARF files for each of the five selected spectra using the *LEMAT* package. A fit on the Crab LECS spectrum shows that 0.8% of systematic plus a fake 2.2 keV Gaussian emission line provide a reduced χ^2 equal to 1. The fake excess around 2.2 keV is, in fact, observed not only in LECS but also in MECS spectra, and is the result of a strong edge-like decrease in the instrument effective area for both instruments, which becomes evident at very high instrument count rates; this excess is *observed in all our five spectra*. While keeping in mind the instrumental issues mentioned above, we added a 0.5% systematic to all instruments; this is a good compromise between taking into account calibration uncertainties and avoiding unreasonably low reduced χ^2 values in the best-fit models. Moreover, we added a Gaussian emission line in the critical edge region (~ 2.2 keV) of LECS and MECS. Another issue at low energies concerns the strong feature observed in the Cyg X-2 LECS spectra (especially in the 1997 data-set) around 1 keV. Since its first detection during a rocket flight in 1971 (Bleeker et al. 1972), several experiments have reported this emission. While from the *Ariel V* data (Branduardi-Raymont et al. 1984) it could not be possible to estimate the line equivalent width (EW) because of the low instrumental sensitivity, *Einstein* observations (Vrtilek et al. 1988) suggested that this feature is likely due to a combination of unresolved Fe L-shell line emission that they identified with Fe XVII, O VIII/Fe XVII, Fe XX/Ni XX and Fe XVII/Fe XXII-XXIV features ranging from 0.74 to 1.12 keV. Also *EXOSAT* observations supported this hypothesis (Chiappetti et al. 1990), although the data did not allow to resolve

this complex region. Based on subsequent measurements with the Broad Band X-ray Telescope (BBXRT) and ASCA, Smale et al. (1993,1994) modeled the excess with a broad Gaussian line having a full width half-maximum (FWHM) and EW in the range ~ 0.05 - 0.33 keV and 8-60 eV, respectively. This modeling provides a good description of the excess also in *BeppoSAX* observations (Kuulkers et al. 1997), resulting in an energy centroid of 1.02 keV, a $\sigma \sim 0.47$ and an EW of 74 eV. By assuming the model proposed by Vrtilik et al. (1988), Kuulkers and co-workers found similar results but differences in EW, thus confirming that the shape of the feature, as well as its EW, changes from observation to observation. However it is worth pointing out that both *Chandra* (Takei et al. 2002) and *XMM-Newton* (Costantini et al. 2005) observations of Cyg X-2 revealed a complex structure of absorption edges (due to combination of N, O, Fe-L, Ne-K shells) in the region 0.4-0.8 keV but no emission around 1 keV. Following the high energy-resolution of these two satellites at low energy and keeping in mind that sometimes the presence of a strong absorption edge, if not taken into account, may give rise of emission-like features in the residuals, we tried to use a single absorption edge in our best-fit models, but the result was completely unsatisfactory requiring actually a Gaussian emission line. Investigating the origin (physical or instrumental) of such 1 keV emission feature is beyond the scope of the present paper and all of the results reported include a Gaussian emission line. Independently from the physical or instrumental origin of the 1 keV emission line, we note that its presences strongly influences the determination of both the interstellar absorption N_{H} and the temperature of the soft BB-like component. In particular, we find that too low N_{H} -values are obtained for the latter parameter ($\sim 0.08 \times 10^{22} \text{ cm}^{-2}$) if compared to results of radio map measurement ($\sim 0.19 \times 10^{22} \text{ cm}^{-2}$: Dickey & Lockman 1990), XMM observations ($\sim 0.18 \times 10^{22} \text{ cm}^{-2}$; Costantini et al. 2005), or *BeppoSAX* observation with no line included ($\sim 0.25 \times 10^{22} \text{ cm}^{-2}$; DS02, F08). The difference of N_{H} are more pronounced in the NB spectra with respect to HB ones: we thus fixed $N_{\text{H}} = 0.15 \times 10^{22} \text{ cm}^{-2}$ for all five analyzed spectra, in order to keep as low as possible this model-dependent variations.

3. Results

The overall continuum of the five spectra was studied using COMPTB³, the newly developed Comptonization model described in detail in F08. Note that while F08 selected different sources in a given spectral state, in this Paper we select a single source and studied its spectral evolution, spanning from the *intermediate* state up to the *soft* state (following the terminology of P06), in order to compare the model parameter evolution during the spectral transition. We remind the reader that Z sources, unlike atolls, have never been detected in the *low/hard* or *hard/PL* state, possibly because they never reach low enough accretion rate levels. Thus the *intermediate* state and the spectral transition to the *soft* state is a complete pattern of the spectral evolution for a Z source.

We briefly remind the reader about the main characteristics of the COMPTB model (Farinelli et al. 2008): the total emerging spectrum is given by

$$F(E) = \frac{C_N}{1+A} (BB + A \times BB * G), \quad (1)$$

where the first and second terms of the right-hand side represent the seed BB-like photon spectrum and its convolution with the system Green's function (Comptonized spectrum), re-

³ The COMPTB model is freely available at web site <http://heasarc.gsfc.nasa.gov/docs/xanadu/xspec/newmodels.html>

spectively. The factor $1/(1 + A)$ is the fraction of the seed photon radiation directly seen by the Earth observer, whereas the factor $A/(1 + A)$ is the fraction of the seed photon radiation up-scattered by the Compton cloud. Free parameters of the model are the BB seed photons color temperature, kT_s and normalization C_N , the plasma temperature, kT_e , the logarithm of the illuminating factor A , $\log(A)$. Moreover, the information on the efficiency of the Comptonization is given by two parameters, α and δ . The parameter α (photon index $\Gamma = \alpha + 1$) indicates an overall Comptonization efficiency related to an observable quantity in the photon spectrum of the data. The lower the α parameter (spectrum extending to higher energies) the higher the efficiency, i.e. the higher energy transfer from hot electrons to soft seed photons. The δ -parameter provides information about the efficiency of bulk BC with respect that to TC. Both α and δ are closely related (see Fig. 1 in F08) and only in the case of a clear cut-off in the hard X-ray tail data is it possible to have a precise estimate of the efficiency of both effects.

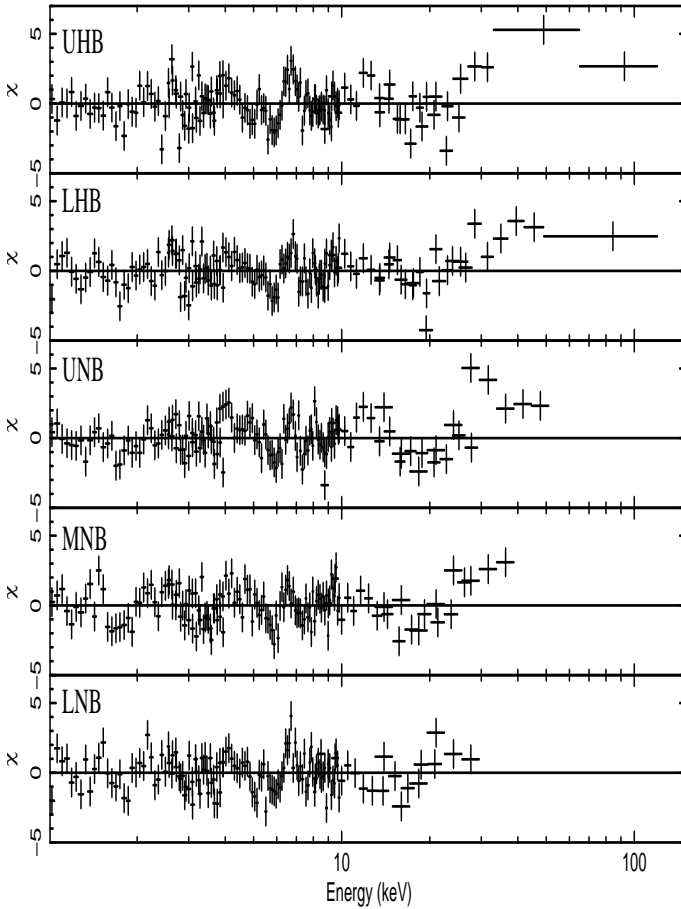


Fig. 3. Residuals in units of σ between the data and best-fit model consisting of a pure TC spectrum (COMPTB with $A \gg 1$) and a simple BB (the latter obtained as COMPTB with $A \ll 1$ and $\delta = 0$). The Gaussian emission lines at ~ 1 and ~ 2.5 keV are also included. The high-energy part (> 20 keV) of the spectrum can be described by simple TC component only at LNB (*lower panel*) but the fit gets progressively worse up towards UHB where systematic deviation of the data is clearly visible.

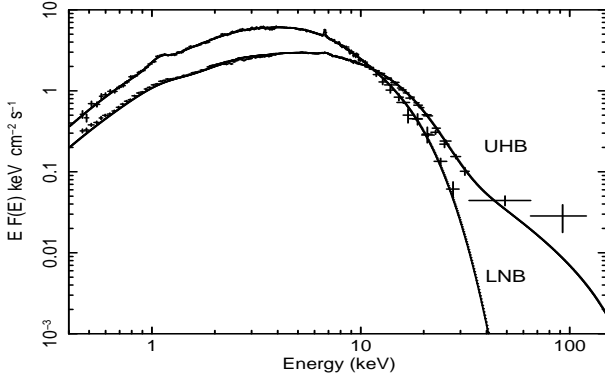


Fig. 4. Unabsorbed $E F(E)$ spectra and best-fit models (see Tab. 1) of the UHB and LNB spectra of Cyg X-2, which show the spectral evolution of the source from its intermediate state (UHB) to the high-soft state (LNB).

Each continuum of the five spectra of Cyg X-2 (two HB and three NB) has been fitted using the sum of two COMPTB components. In Tab. 1 we report the results of our spectral analysis. In all cases, the first COMPTB component [pure TC ($\delta=0$)] provides a significant contribution in the total emerging spectrum. Most of the source energetic budget (60-70 %) is, in fact, determined by this component which is described (a well-known feature of Z-class LMXBs) by Comptonization of ~ 0.3 keV photons off cool electrons ($kT_e \sim 3-5$ keV) of high optical depth environment ($\tau \sim 10$ or 5 depending on the geometry of the cloud, sphere or slab, respectively). The direct seed BB-like spectrum is not seen in this case because of the high optical thickness of the Compton cloud. We note that the BB temperature at UHB stage is a factor about two higher than the value reported in F08 for the same data set. This is due to the fact that here we included a Gaussian emission line at 1 keV which, as already stated in Section 2, may affect both the estimated interstellar absorption N_H and the parameters of low-energy continuum features.

In addition to the dominating TC component, broad-band spectra of high-luminosity LMXBs also show the presence of a ~ 1 keV BB-like component whose origin is generally claimed to be close to the NS surface. This low-energy component is included in our spectra with a second COMPTB model which, in fact, takes into account the presence of a directly visible BB-like spectrum (see Eq. 1). In all five spectra there is also an evidence of a Gaussian emission line around 6.7 keV. We note however that this continuum model (TC plus BB) provides accurate description of the data only for the spectrum at LNB stage, while a systematic excess above $\gtrsim 20$ keV is observed mainly at UHB and LHB with decreasing strength of this excess at UNB and MNB (see Fig. 3). This systematic deviation of data from the typical soft state continuum model is, in fact, the well-known high-energy transient behaviour of some LMXBs, including Cyg X-2 (see also DS02).

In general this high-energy feature can be fitted with a simple PL, but in the context of the more physical approach to the X-ray spectral formation one can treat it as a BC emission (see the second term in Eq. [1], $BB * G$, of COMPTB). The latter describes the result of Comptonization of a seed photon population by a medium subjected to inward bulk motion so that both TC and BC contribute to the emergent spectrum. In this case it is necessary to introduce additional free parameters aimed to describe the physical properties of the bulk region, namely α , δ , kT_e and $\log(A)$.

However, if the number of free parameters describing the high energy part of the X-ray spectrum (i.e. the second COMPTB in Tab. 1) exceeds the number of observable quantities (PL slope,

normalization and spectral cut-off), degeneracy of the parameters (impossibility to constrain them) occurs and some assumptions have to be made in order to reduce the free-parameter space dimension. As the first of our assumptions we suggest that the Comptonizing plasma temperature of the two COMPTB models are equal each other (see Tab. 1). In fact as already pointed out by F08 there is no expectation of some strong electron temperature variation in the region extending from the outer TC medium up to the innermost bulk region. The lack of an unambiguous rollover ($\gtrsim 100$ keV) in the high-energy data reduces the number of measurable spectral characteristics of the high-energy transient X-ray emission, which are essentially the PL slope and its normalization. The latter quantity is expressed through $\log(A)$ in the model, while the spectral index α provides the spectral slope. For a given fixed value of α , when the bulk parameter δ increases, the high-energy cut-off energy increases too, leading to the extension of the PL-like component in the spectrum (see Fig. 1 in F08).

The statistics of the spectral data at UHB and LHB stages did not allow us to simultaneously constrain α , $\log(A)$ and δ . Since we are mainly interested in studying the importance of BC as a function of the source position in the Z-track, this mapping was possible only leaving free the bulk parameter δ and fixing the energy index α . A detailed study of the parameter space showed us that the minimum of the χ^2 could be obtained by fixing $\alpha=2.5$. The results obtained with this modeling approach are reported in Tab. 1. One can see that only the lower limit (at 90% confidence level) on $\log(A)$ can be determined in both HB spectra, while as far as δ is concerned, we have a lower limit for its value at UHB and better constrain of this at LHB. The situation gets even more critical for the parameter determination of the NB spectra. In the UNB and MNB cases, where a high-energy excess is still observed over the BB plus TC continuum (see Fig. 3) it was not possible to put serious constraints on both δ and $\log(A)$ leaving them simultaneously free, mainly because of the lack of counts at high energies. The only possibility to explore the behaviour of δ was thus fixing $\log(A)$ at the best-fit value of the LHB spectrum (see Tab. 1). Finally, in the LNB spectrum the second COMPTB model requires neither thermal nor bulk Comptonization, resulting in a simple BB shape. The overall LNB spectrum could hence be well fit by the sum of thermal Comptonization (the first COMPTB) plus a BB. In terms of best-fit improvement, the addition of the TC component to the BC one gives $\Delta\chi^2 \sim 100$ (F-test $\sim 10^{-17}$) and $\Delta\chi^2 \sim 63$ (F-test $\sim 10^{-10}$) for the UNB and MNB spectra, respectively, while for the LNB spectrum it is only $\Delta\chi^2 \sim 19$ (F-test $\sim 10^{-4}$).

4. Discussion

We have studied newly extracted Cyg X-2 *BeppoSAX* spectra, covering the horizontal and normal branch of the Z-track, using the COMPTB model recently developed by Farinelli et al. (2008). We remark that COMPTB is a Comptonization model that includes both TC and BC, namely it can be considered as an (updated) merging of the well known COMPTT and BMC XSPEC models.

4.1. Interpretation of the observed spectra

We have fitted the continuum of all the five source spectra with two COMPTB models. The first one represents the dominating TC component of the spectrum, while the second one provides description of the strong ~ 1 keV BB-like feature and, when observed, the hard X-ray emission

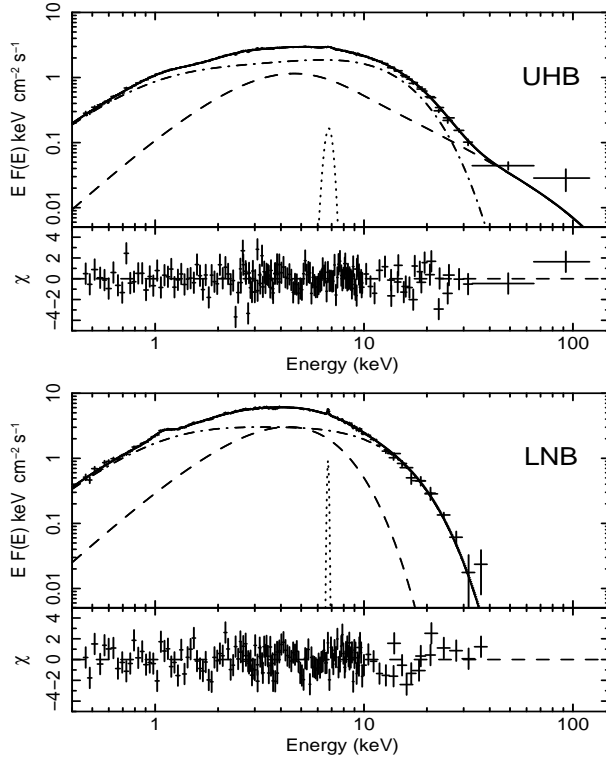


Fig. 5. Unabsorbed $EF(E)$ spectra, best-fit model and residuals between data and model in units of σ for the UHB and LNB spectra of Cyg X-2. Different line styles represent single component of the best-fit model reported in Tab. 1. *Dotted-dashed*: COMPTB with pure TC. *Long-dashed*: COMPTB which includes TC and BC, i.e. $\delta \gg 1$ (*left panel*) or with simple BB spectrum (*right panel*). *Dotted*: Gaussian emission line.

above 30 keV. In our scenario (see also F07 and F08), the thermal COMPTB component is an emission originated in the relatively cold (~ 3 keV) and optically thick ($\tau \sim 5$) outer transition layer due to the Comptonization of cold disk seed photons (~ 0.3 keV). This component is rather stable as can be seen in Tab. 1. The second COMPTB component originates in the innermost region of the system and is subjected to major changes (Tab. 1). Hot BB photons (~ 1 keV) are emitted by the neutron star surface and within the transition layer itself. The spectral shape variability is due to the changing Comptonization of this seed photon population, mainly led by the accretion rate, as discussed Section 4.2. The difference in the measured values of kT_s (a factor about three) strongly points in favour of two distinct populations of seed photons, which in turn translates in the existence of two physically separated regions. Looking at the best-fit parameters in Tab. 1, the source spectral stability of the persistent continuum is almost evident, in general agreement with high-luminosity LMXBs properties. Moreover, in the MNB and LNB spectra, the TC parameter are also well constrained, differently from what reported in DS02 where they strongly deviate from a smooth trend with unreasonable associated errors. We claim that one reason of the DS02 results could be the rough timing selection for spectral analysis (see Section 2). The quantity that undergoes the major change as a function of the source position in the CD/HID is in fact the estimated 0.1–200 keV luminosity which has a maximum increase of about 80% from the UHB to the UNB-MNB state. Less significant variations are observed in the plasma temperature kT_e and the thermal component *Comptonization amplification factor* (CAF), defined as the ratio

of energy fluxes of Comptonized over seed photons. The CAF, in fact, decreases monotonically from the UHB to the LNB. We also observe that the inferred plasma temperature, optical depth and luminosity in the LNB slightly deviates from the monotonic trend seen in the first four spectra. Whether this small jump is real or due to some bias in the spectral modeling is not straightforward. In particular the presence of a strong 1 keV and weaker 2.5 keV emission feature especially in the NB spectra may play some role in the actual determination of the temperature of the seed photons of the pure thermal COMPTB model, which is reflected in the kT_e and α values.

4.2. Spectral evolution as a function of mass accretion rate

The new theoretical and observational support provided in the last years (e.g., TMK97, P06, F08) to the study of hard X-ray emission in LMXBs significantly pushed forward our knowledge about the nature of the emission processes in these sources. Multi-wavelength observations of Z sources (e.g., Pennix et al. 1988; Vrtilik et al. 1990) strengthened the evidence that the motion of the sources along the Z track is mainly controlled by the accretion rate \dot{M} which increases from the HB to the FB. However, little is said on why an increase in \dot{M} leads to a disappearance of the hard tail in LMXBs and, moreover, the actual meaning of \dot{M} itself is not fully understood. It is however widely accepted that the simple source bolometric X-ray luminosity is not a good \dot{M} -tracer, a hint occurring not only in NS but also in black hole (BH) systems (e.g., van der Klis 2001). We propose to actually define *two* \dot{M} -values for a single source, one related to the accretion disk \dot{M}_{disk} and another one (\dot{M}_{tl}) to the so-called transition layer (TL), the region where the disk angular velocity deviates from its Keplerian rotation in order to adjust to the angular velocity of the slowly spinning NS. The reason for this splitting is that at very high accretion rate levels (close to the Eddington limit), the radiation pressure from the accretion disk may eject a significant fraction of the accreted matter, producing a powerful wind surrounding the system (Bradshaw et al. 1997). In this case the mass flow coming from the innermost part of the disk through the TL to the NS surface is less than that arriving at the disk outer part, namely $\dot{M}_{\text{tl}} \lesssim \dot{M}_{\text{disk}}$, with $\dot{M}_{\text{tl}} \propto \dot{M}_{\text{disk}}$ (Titarchuk et al. 2007b).

Focusing the attention to the TL region, it is worth noting that both theoretical (TMK96, TMK97) and extended data analysis works (P06, F07, F08) led to the possibility that the bulk Comptonization process in the TL is responsible for the hard X-ray emission in NS LMXBs. A self-consistent physical treatment of the TL region is presently being developed by Titarchuk & Farinelli (2008, in preparation, hereafter TF08); the numerical solution of the radial momentum equation performed by FT08 unambiguously shows that matter arriving at the *transition radius* from the Keplerian disk with some fraction of the characteristic disk radial (magneto-acoustic) velocity and then it proceeds through the transition layer towards the NS with an almost constant velocity up to some radius over which it further proceeds in quasi free-fall manner, getting the NS surface with $V_R \sim 0.1c$. However, as FT08 emphasize, this free-fall region *is not always present* but it depends on *the mass accretion rate* \dot{M} , which can thus be now identified with \dot{M}_{tl} . In particular, high \dot{M}_{tl} generates a strong radiation field in the TL whose pressure gradient prevents matter from reaching the NS surface with the high-speed which is necessary to produce, via Doppler effect, hard X-ray photons (hence no hard tail detected). We remind once again the reader that the

only observable quantities in the high-energy X-ray spectra are the PL photon index $\gamma = \alpha + 1$, its normalization and the high-energy cut-off, if detected. The actual accretion rate (regardless its definition) is not a directly measurable quantity; its estimation can be done only including it as a free parameter in devoted accretion models. This is, e.g., what has been done by Becker & Wolff (2007) in their model for accretion columns in X-ray pulsars. On the other hand, in COMPTB the accretion rate is not a free parameter, it is just somewhat implicitly hosted in the bulk parameter as $\delta \propto \dot{m}^{-1}$ (where $\dot{m} \equiv \dot{M}/\dot{M}_{\text{Edd}}$, F08). We also note that in the *intermediate state* spectra of NS LMXBs, *two spectral indexes* are actually observed in the X-ray spectrum, the first one related to pure TC and the second one to a mixed thermal-bulk Comptonization effect.

For Cyg X-2, in the former case the spectral index $\alpha \sim 1$ (see Tab. 1) which is typical for the intermediate state in NS sources⁴. As far as the second spectral index is concerned, it is important to discuss the differences between systems hosting a NS or a BH. For BH sources, subjected to enhanced spectral transitions, in fact just *one* index is measured in the spectrum. It evolves from $\alpha \sim 1.7$ in hard state, which is TC-dominated with observed cut-off around 100 keV, to $\alpha \sim 2.8$ in the BC-dominated soft state. In this BC case, *index saturation* is observed (Shaposhnikov & Titarchuk 2008). In fact, it can be proven (Bradshaw et al. 1997) that $\alpha \approx Y^{-1}$, where the Comptonization parameter $Y = \eta N_{\text{sc}}$, η is the average energy exchange per scattering and N_{sc} is the average number of scatterings. In a BC-dominated flow, $\eta \propto \tau^{-1}$ and $N_{\text{sc}} \propto \tau$ (Laurent & Titarchuk 2007) so that saturation occurs. But this actually occurs in BH systems, where the presence of a fully absorption inner boundary condition for the radiation (TMK97) allows bulk motion to be always present. In the case of NS system, the presence of a solid surface (reflection boundary condition) plays a crucial role, given that the radiation pressure gradient gets increasing with the accretion rate until bulk flow is stopped. Thus no index saturation can be observed in NS sources. The innermost part of the system evolves towards thermal equilibrium when the emergent spectrum consists of two blackbody-like components which are related to NS surface and disk emissions (Titarchuk & Shaposhnikov 2005).

On the basis of these considerations we may tentatively discuss the parameters behaviour reported in Tab. 1: along the horizontal branch (HB), at lower \dot{M} level, BC effect can efficiently pronounced as it is indicated by the high δ -value. A slight decrease of the BC effect is observed in the spectra in the low part of HB (LHB), where both δ and $\log(A)$ get lower, even though this effect seems to be marginal given the high error bars for both these parameters. The total (0.1-200 keV) source luminosity at LHB increases about 20% with respect to that at UHB. When the sources is at the UNB (upper normal branch), a further increase ($\sim 50\%$) of the luminosity with respect to that at LHB occurs, accompanied by significant decrease of the hard X-ray emission (see Fig. 3). We may interpret this behaviour as an increase of \dot{M}_{disk} which in turn leads to higher \dot{M}_{tl} and consequently leads to the increase of the radiation pressure in the TL. This pressure works against an inward matter motion and the bulk effect decreases (though it may be still present but below the instrument threshold). Figure 4 illustrates this spectral transition, due to \dot{M} change, from the intermediate (UHB) to soft (NB) state, following the terminology defined in P06.

In the spectrum the power-law extension reduces as a result of the BC efficiency (δ -parameter) reduction. Looking at the parameters of Tab. 1 and at the residuals in Fig. 3 it is possible to see

⁴ This result can be verified from the best-fit values of kT_e and τ obtained from COMPTT in previous works (see references in Section 1) and using Eqs. [17] and [24] in TL95.

that the situation only slightly changes at MNB. Finally, in the LNB no hard X-ray emission is observed and a simple BB-like spectrum along with the TC bump is present. It is possible that at this stage the effect of radiation pressure in the TL is strong enough in stopping bulk motion, or at least bringing its visible effect below the instrument threshold. At this stage it is very likely that matter follows a very complex behaviour; it may arrive at the NS surface very slowly or it may significantly spread over the stellar surface (Inogamov & Sunyaev 1999) producing additionally a thick layer which suppresses the radio emission (P06).

Note however that the 0.1-200 keV luminosity at LNB is about 12% lower than that at UNB and MNB. These results clearly demonstrates that the X-ray luminosity is not a good tracer of the accretion rate, whatever one defines it. In all five spectra, a direct BB-like component, providing about 25% of the source energetic budget, is observed (indeed in the second COMPTB component, $\log(A)$ is small in all cases). The estimated BB *color radius* in all cases is $R_{\text{bb}} \lesssim 5$ km; while this value has to be treated very carefully (it is derived from the measured BB *color temperature* kT_s assuming isotropic emission) its order of magnitude is consistent with the NS radius, pointing to an origin close to the compact object surface. In our interpretation, these BB-like seed photon spectra have origins related to the thermal emissions of the NS surface and to local energy release emission in the TL region. It is possible that part of this soft component is direct radiation from the seed photon region (NS or TL) and the other one consists of photons which are not affected by the Comptonization. The fraction of this directly escaping radiation is parameterized through $\log(A)$ related to both a geometrical (covering factor) and spatial (seed photon distribution) system configuration in the innermost part, even though the relative importance among the two effects cannot be determined from the X-ray spectrum.

5. Conclusions

The scenario where both thermal and bulk Comptonization contribute to explain the LMXB spectral evolution is gaining strong theoretical (TMK96, TMK97, Laurent & Titarchuk 1999, 2001, TF08) and observational support (Shrader & Titarchuk 1998; Borozdin et al. 1999, P06, F07, F08, this paper). This is true also for the case of accretion powered X-ray pulsars for which a new theoretical model based on thermal and bulk Comptonization occurring in the accreting shocked gas has been recently presented (Becker & Wolff 2007). In the model presented by Becker & Wolff (2007), the effects of the strong magnetic field ($B \sim 10^{12}$ G) become very important and are included, whereas in this paper we have used a model that has been recently proposed by F08 to study low-magnetized compact objects ($B \lesssim 10^9$ G), where effects of the magnetic field within the flow can be neglected (as opposed to the radiation pressure). The two models are complementary and we believe they can be an important step forward to understanding and relating the physics of bursting (low- B) and pulsating (high- B) accreting NSs. Nevertheless the present analysis has revealed the key importance of having a next generation of very high-sensitivity missions at energies extending up to 300-400 keV. The detection of high-energy cut-off in extended PL-like tails of both NS and BH binary systems would be one breakthrough in understanding the physics of accretion processes very close to the compact object, providing constraints on the bulk energy of the matter.

Acknowledgements. The authors are very grateful to the anonymous referee, whose suggestions strongly improved the quality of the paper with respect to the formerly submitted version. AP acknowledges the Italian Space Agency financial

and programmatic support via contract I/008/07/0. This work has been partially supported by the grant from Italian PRIN-INAF 2007, "Bulk motion Comptonization models in X-ray Binaries: from phenomenology to physics", PI M. Cocchi.

References

- Asai, K., Dotani, T., Mitsuda, K., et al. 1994, PASJ, 46, 479
- Barret, D. 2001, *Advances in Space Research*, 28, 307
- Becker, P. A. & Wolff, M. T. 2007, *ApJ*, 654, 435
- Bleeker, J. A. M., Deerenberg A. J. M., Yamashita, K., et al. 1972, *ApJ*, 178, 377
- Boella, G., Butler, R. C., Perola, G. C., et al. 1997a, *A&AS*, 122, 299
- Boella, G., Chiappetti, L., Conti, G., et al. 1997b, *A&AS*, 122, 327
- Borozdin, K., Revnivtsev, M., Trudolyubov, S., Shrader, C., & Titarchuk, L. 1999, *ApJ*, 517, 367
- Bradshaw, C.F., Titarchuk, L., & Kuznetsov, S. 2007, *ApJ*, 663, 1225
- Branduardi-Raymont, G., Ercan, E. N., & Chiappetti, L. 1984, *A&A*, 130, 175
- Chiappetti, L., Treves, A., Branduardi-Raymont, G., et al. 1990, *apj*, 361, 596
- Costantini, E., Freyberg, M. J., & Predehl, P. 2005, *A&A*, 444, 187
- D'Amico, F., Heindl, W. A., Rothschild, R. E., & Gruber, D. E. 2001, *ApJ*, 547, L147
- Dickey, J.M. & Lockmann, F.J. 1990, *ARA&A*, 28, 215
- Di Salvo, T., Farinelli, R., Burderi, L., et al. 2002, *A&A*, 386, 535
- Di Salvo, T., Goldoni, P., Stella, L., et al. 2006, *ApJ*, 649, L91
- Di Salvo, T., Robba, N. R., Iaria, R., et al. 2001, *ApJ*, 554, 49
- Di Salvo, T. & Stella, L. 2002, in Proc. of the XXXVIIth Rencontres de Moriond, *The Gamma-Ray Universe*, Ed. A. Goldwurm, Doris N. Neumann and Jean Tran Thanh Van, 67
- Di Salvo, T., Stella, L., Robba, N. R., et al. 2000, *ApJ*, 544, L119
- Falanga, M., Götz, D., Goldoni, P., et al. 2006, *A&A*, 458, 21
- Farinelli, R., Frontera, F., Zdziarski, A. A., et al. 2005, *A&A*, 434, 25
- Farinelli, R., Titarchuk, L., & Frontera, F. 2007, *ApJ*, 662, 1167 (F07)
- Farinelli, R., Titarchuk, L., Paizis, A., & Frontera, F. 2008, *ApJ*, 680, 602, (F08)
- Frontera, F., dal Fiume, D., Malaguti, G., et al. 1998, in *The Active X-ray Sky: Results from BeppoSAX and RXTE*, ed. L. Scarsi, H. Bradt, P. Giommi, & F. Fiore, p. 286
- Frontera, F., Costa, E., dal Fiume, D., Feroci, M., Nicastro, L., Orlandini, M., Palazzi, E., & Zavattini, G. 1997, *A&AS*, 122, 357
- Hasinger, G., van der Klis, M., Ebisawa, K., Dotani, T., & Mitsuda. 1990, *A&A*, 235, 131
- Inogamov, N.A., & Sunyaev, R.A. 1999, *ApJ*, *AstL*, 25, 269
- Kuulkers, E., Parmar, A. N., Owens, A., Oosterbroek, T., & Lammers, U. 1997, *A&A*, 323, 29
- Laurent, P., & Titarchuk, L. 2007, *ApJ*, 656, 1056
- Laurent, P., & Titarchuk, L. 2001, *ApJ*, 562, L67
- Laurent, P., & Titarchuk, L. 1999, *ApJ*, 511, 289
- Lavagetto, G., Iaria, R., di Salvo, T., et al. 2004, *Nuclear Physics B, Proceedings Supplements*, 132, 616
- Ling, J. C., Wheaton, W. A., Mahoney, W. A., et al. 1996, *A&AS*, 120, 677
- Maurer, G. S., Johnson, W. N., Kurfess, J. D., & Strickman, M. S. 1982, *ApJ*, 254, 271
- Mitsuda, K., Inoue, H., Koyama, K., et al. 1984, PASJ, 36, 741
- Nishimura, J., Mitsuda, K., & Itoh, M. 1986, PASJ, 38, 819
- Paizis, A., Ebisawa, K., Tikkanen, T., et al. 2005, *A&A*, 443, 599
- Paizis, A., Farinelli, R., Titarchuk, L., et al. 2006, *A&A*, 459, 187 (P06)
- Penninx, W., Lewin, W.H.G., Zijlstra, A.A., Mitsuda, K., & van Paradijs, J. 1988, *Nature*, 336, 146
- Peterson, L. E. 1973, in *IAU Symposium*, Vol. 55, X- and Gamma-Ray Astronomy, ed. H. Bradt & R. Giacconi
- Smale, A. P., Done, C., Mushotzky, R. F., et al. 1993, *ApJ*, 410, 796
- Smale, A. P., Angelini, L., White, N. E., Mitsuda, K., & Dotani, T. 1994, *BAAS*, 26, 1484
- Shrader, C., & Titarchuk, L. 1998, *ApJ*, 499, L31
- Shakura, N. I., & Sunyaev, R. A. 1973, *â*, 24, 337
- Takei, Y., Fujimoto, R., Mitsuda, K., & Onaka, T. 2002, *ApJ*, 581, 307

- Titarchuk, L., & Lyubarskij, Y. 1995, *ApJ*, 450, 876
- Titarchuk, L., Mastichiadis, A., & Kylafis, N. D. 1996, *A&AS*, 120, 171
- Titarchuk, L., Mastichiadis, A., & Kylafis, N. D. 1997, *ApJ*, 487, 834
- Titarchuk, L., & Fiorito, R. 2004, *ApJ*, 612, 988
- Titarchuk, L., & Shaposhnikov, N. 2005, *ApJ*, 626, 298
- Titarchuk, L., Kuznetsov, S., & Shaposhnikov, N. 2007a, *ApJ*, 667, 404
- Titarchuk, L., Shaposhnikov, N., & Arefiev, V. 2007b, *ApJ*, 660, 556
- van der Klis, M. 2001, *ApJ*, 561, 943
- Vrtilek, S. D., Swank, J. H., & Kallman, T. R. 1988, *ApJ*, 326, 186
- Vrtilek, S.D., Raymond, J.C., Garcia, M. R., Verbunt, F., Hasinger, G., & Kurster, M. 1990, *A&A*, 235, 162
- White, N. E., Peacock, A., Hasinger, G., et al. 1986, *MNRAS*, 218, 129
- Winkler, C., Courvoisier, T. J.-L., Di Cocco, G., et al. 2003, *A&A*, 411, L1

Table 1. Best-fit parameters of the multi-component model WABS(COMPTB + COMPTB + Gaussian). Errors are computed at 90% confidence level for a single parameter. Additional emission lines at ~ 1 keV and ~ 2.5 keV were included in all the five spectra (see Section 2).

Parameter	UHB	LHB	UNB	MNB	LNB
N_{H}^{a}	[0.15]	[0.15]	[0.15]	[0.15]	[0.15]
COMPTB (thermal: $\log A = 8, \delta=0$)					
kT_{s} (keV)	$0.28^{+0.02}_{-0.03}$	$0.29^{+0.02}_{-0.02}$	$0.31^{+0.01}_{-0.01}$	$0.30^{+0.01}_{-0.01}$	$0.31^{+0.01}_{-0.01}$
kT_{e} (keV)	$2.72^{+0.06}_{-0.08}$	$2.65^{+0.08}_{-0.10}$	$2.41^{+0.04}_{-0.04}$	$2.23^{+0.06}_{-0.05}$	$2.51^{+0.06}_{-0.08}$
α	$0.80^{+0.03}_{-0.03}$	$0.82^{+0.07}_{-0.03}$	$0.80^{+0.03}_{-0.03}$	$0.82^{+0.04}_{-0.04}$	$1.00^{+0.08}_{-0.02}$
τ^{b}	6.5	6.4	6.9	7.1	5.8
CAF ^c	2.8	2.6	2.5	2.4	2.2
COMPTB					
kT_{s} (keV)	$1.00^{+0.08}_{-0.11}$	$1.15^{+0.05}_{-0.14}$	$1.11^{+0.02}_{-0.02}$	$1.08^{+0.03}_{-0.03}$	$1.16^{+0.03}_{-0.04}$
R_{bb}^{d} (km)	3.4	3.2	4.6	4.9	4.6
kT_{e} (keV)	[kT_{e}]	[kT_{e}]	[kT_{e}]	[kT_{e}]	-
$\log(A)$	0.11 (>-0.12)	-0.40 (>-0.65)	[-0.4]	[-0.4]	[-8]
α	[2.5]	[2.5]	[2.5]	[2.5]	-
δ	75 (>40)	49^{+39}_{-18}	25^{+5}_{-4}	22^{+5}_{-4}	-
Gaussian					
E_{l} (keV)	$6.76^{+0.09}_{-0.08}$	$6.74^{+0.11}_{-0.12}$	$6.74^{+0.09}_{-0.09}$	$6.63^{+0.13}_{-0.11}$	$6.72^{+0.10}_{-0.08}$
σ_{l} (keV)	$0.3^{+0.2}_{-0.1}$	0.16 (< 0.33)	$0.10^{+0.17}_{-0.10}$	$0.12^{+0.19}_{-0.12}$	0.06 (< 0.25)
I_{l}	$2.5^{+0.9}_{-0.7}$	$1.38^{+0.73}_{-0.55}$	$1.94^{+0.71}_{-0.65}$	$1.83^{+0.95}_{-0.78}$	$3.00^{+1.73}_{-0.91}$
EW_{l} (eV)	38^{+18}_{-9}	17^{+8}_{-8}	15^{+5}_{-5}	14^{+7}_{-6}	29^{+16}_{-9}
$L_{\text{bb}}^{\text{e}}/L_{\text{tot}}$	0.25	0.26	0.25	0.25	0.28
$L_{\text{th}}^{\text{f}}/L_{\text{tot}}$	0.69	0.67	0.63	0.61	0.63
$L_{\text{tot}}^{\text{g}}$	0.9	1.1	1.7	1.7	1.5
χ^2/dof	175/152	162/154	159/148	185/144	197/143

^a In units of 10^{22} cm^{-2} .

^b Computed from kT_{e} and α using equations [17] and [24] for slab geometry in Titarchuk & Lyubarskij (1995).

^c Compton Amplification Factor (see text for the definition).

^d Computed using the simple relation $L = 4\pi\sigma R^2 T^4$.

^e Ratio between the direct BB component flux of the second COMPTB and the total flux in the 0.1-200 keV energy range.

^f Ratio between the TC component flux and the total flux in the 0.1-200 keV energy range.

^g In units of $10^{38} \text{ erg s}^{-1}$ computed in the energy range 0.1–200 keV assuming a source distance of 8 kpc.